

# The spectroscopic characteristics of intermediate-aged pre-main sequence stars: the $\eta$ Chamaeleontis cluster

A-Ran Lyo,<sup>1,2\*</sup> Warrick A. Lawson<sup>1\*</sup> and M. S. Bessell<sup>3\*</sup>

<sup>1</sup>*School of PEMS, The University of New South Wales, Australian Defence Force Academy, Canberra, ACT 2600, Australia*

<sup>2</sup>*Institute of Astronomy and Astrophysics, Academia Sinica, P. O. Box 23-141, Taipei 106, Taiwan*

<sup>3</sup>*RSAA, Institute of Advanced Studies, The Australian National University, Cotter Rd, Weston Creek, ACT 2611, Australia*

Accepted 16 August 2004

## ABSTRACT

We present a study of calibrated low-resolution spectra of the 18 known primaries of the  $\approx 9$  Myr-old  $\eta$  Chamaeleontis pre-main sequence (PMS) star cluster. Using synthetic broadband colours and narrow-band continuum-, temperature- and gravity-sensitive indices derived from the spectra, we compare the  $\eta$  Cha stars to standard dwarfs. We find that the *VRI* colours of the PMS stars are indistinguishable from those of main-sequence stars, but that a *B*-band excess attaining  $\approx 0.2$  magnitudes for late-M cluster stars is present that might be an indicator of gravity, metallicity and/or activity differences between the two samples of stars. The narrow-band spectral indices for the  $\eta$  Cha stars possibly indicate higher metallicity and strongly indicate lower surface gravity than the dwarf indices, consistent with the elevated location of the cluster in the Hertzsprung-Russell (H-R) evolutionary diagram. Using the derived synthetic colours and indices, we adopt spectral types for the late-type  $\eta$  Cha stars, and then produce a table of absolute optical magnitudes and colours representing the cluster isochrone for comparison with PMS evolutionary models. From our results we also conclude that the  $\eta$  Cha stars are unreddened, consistent with the group being a sample of older PMS stars distant from obscuring molecular clouds, except for the A1 member HD75505 for which we confirm  $A_V = 0.4$  magnitudes likely due to the presence of circumstellar material.

**Key words:** stars: pre-main-sequence — stars: fundamental parameters — open clusters and associations: individual:  $\eta$  Chamaeleontis

## 1 INTRODUCTION

Stellar spectroscopy is an indispensable tool in the study of stellar structure and evolution. By comparing spectra of individual stars or the members of cluster/groups with spectra of standard stars with well defined properties, estimates can be made of temperature, luminosity and composition, i.e. effective temperature *via* spectral types, stellar luminosity *via* effective gravity sensitive indicators and chemical composition *via* metallicity/abundance indicators. Bessell (1991) has presented some details for M-type stars.

For PMS populations, studies show that the overall spectroscopic characteristics of PMS stars and brown dwarfs are similar to those of main sequence stars and field brown dwarfs but with detailed differences in key atomic and molecular lines, e.g. Martín, Rebolo & Zapatero-Osorio

(1996) found the gravity-sensitive K I and Na I lines are weaker in young Pleiades brown dwarfs than in field objects of similar spectral type, while Mohanty et al. (2004) demonstrated the gravity-sensitivity of the TiO molecular bands, which increase in strength with decreasing effective gravity, in samples of PMS stars in Upper Scorpius and Taurus star-forming regions. The differences in these features are relevant to all young PMS populations, with ages several-Gyr less than old-disk dwarfs and elevated in the H-R diagram by several magnitudes above the main-sequence.

Nearby young clusters have distinct advantages for the study of fundamental properties of PMS stars. They provide a sample of stars across a wide range of spectral types at essentially uniform age, distance and metallicity, and are sufficiently bright for precise spectroscopic characterization. Our laboratory is the  $\approx 9$  Myr-old  $\eta$  Chamaeleontis cluster (Mamajek, Lawson & Feigelson 1999). The cluster is an ideal PMS group for the study of ‘intermediate-aged’ PMS stars owing to its well-defined distance from *Hipparcos* mea-

\* E-mail: arl@asiaa.sinica.edu.tw (A-RL); wal@ph.adfa.edu.au (WAL), bessell@mso.anu.edu.au (MSB)

surements ( $d = 97 \pm 3$  pc), compactness (extent  $\sim 1$  pc), the apparent high degree of coevality of the stellar population, and location distant from obscuring molecular clouds (Majajek, Lawson & Feigelson 2000; Lyo et al. 2004).

In this paper, we investigate in detail the spectroscopic characteristics of the stellar population of the  $\eta$  Cha cluster using calibrated low-resolution spectra, and compare these PMS stars to main-sequence stars across the range of spectral types present in the cluster.

## 2 OBSERVATIONS AND DATA REDUCTION

### 2.1 Calibration of the spectra

We obtained low-resolution spectra of most members of the  $\eta$  Cha cluster and calibration stars during 2002 March using the 2.3-m telescope and double beam spectrograph (DBS) at Mount Stromlo and Siding Spring Observatories (MSSSO). Using the same equipment, several other calibration stars were observed during 2003 April, and an additional low-mass cluster member discovered by Song, Zuckerman & Bessell (2004) was observed during 2004 January. The observing log for the cluster members is summarized in Table 1. For comparison with the late-type cluster stars, we obtained DBS spectra for main-sequence K- and M-type dwarfs from the Gliese catalogue; see Bessell (1990) for a list of Gliese stars with photoelectric photometry and spectral types. To investigate the spectral types of the three early-type cluster members, we also obtained DBS spectra of several B- and A-type dwarfs from the Bright Star Catalog.

For each star, spectra were obtained simultaneously in the blue and red arms of the DBS in a pseudo-spectrophotometric mode, with the slit width set to maximise the spectral resolution and oriented to the parallactic angle to eliminate differential refraction. In the blue arm, the 300B (300 line  $\text{mm}^{-1}$ ) grating yielded spectra with a resolution of 4 Å (2 pixels) with wavelength coverage from  $\lambda\lambda 3000 - 6000$  Å. In the red arm, the 158R (158 line  $\text{mm}^{-1}$ ) grating yielded spectra with a resolution of 8 Å (2 pixels) with wavelength coverage from  $\lambda\lambda 5000 - 11000$  Å.

The spectra were first reduced using dome flats, bias frames and Ne-Ar arc frames after removing cosmic rays (using the automatic IRAF cosmic ray routine, or manually using `imedit`) and making use of standard IRAF library routines such as `ccdproc` and `apall`.

Then a ‘smooth-spectrum’ source was used to produce a division template for all objects (programme stars and spectrophotometric flux standards) observed during any given night at the same grating settings. Prior to the division operation, any strong stellar lines present in the template spectrum were manually removed using editing options within `plot`, e.g. H and He lines in the blue, and  $\text{H}\alpha$ , the Na D lines and the infrared Ca II triplet in the red. The template spectrum was then smoothed to effectively increase the signal-to-noise ratio, prior to the division process which serves to remove the first-order telluric absorption and large-scale instrumental variations along the spectrum due to detector sensitivity, grating efficiency, and spectrograph vignetting. However, the telluric absorption is not constant with time. Some of the bands, particularly the  $\text{O}_2$  bands, are almost saturated, but the  $\text{H}_2\text{O}$  bands are only partially saturated

**Table 1.** Observing log for the  $\eta$  Cha cluster stars, listed in order of observation. Throughout this paper, we identify the late-type stars by their RECX or ECHA number. (In this table, we also list their variable star designation, where applicable). The three early type stars are identified by their common name (with their RECX number listed where applicable). The UT date refers to the time of mid-exposure for the red-beam (158R grating) observation.

Star	UT date	Exp. (s) (300B)	Exp. (s) (158R)
RECX 1 (EG Cha)	2002 Mar 24.4014	300	60
$\eta$ Cha (RECX 2)	2002 Mar 24.4077	3	1
HD 75505	2002 Mar 24.4099	15	5
RS Cha (RECX 8)	2002 Mar 24.4122	5	2
RECX 7 (EM Cha)	2002 Mar 24.4146	300	60
RECX 11 (EP Cha)	2002 Mar 24.4203	180	90
RECX 10 (EO Cha)	2002 Mar 24.4247	180	180
RECX 4 (EI Cha)	2002 Mar 24.4289	300	180
RECX 12 (EQ Cha)	2002 Mar 24.4344	300	180
ECHA J0843.3-7905	2002 Mar 24.4427	600	300
RECX 3 (EH Cha)	2002 Mar 24.4552	600	600
RECX 6 (EL Cha)	2002 Mar 24.4643	600	600
RECX 9 (EN Cha)	2002 Mar 24.4734	600	600
RECX 5 (EK Cha)	2002 Mar 24.4827	600	600
ECHA J0841.5-7853	2002 Mar 24.4912	600	600
ECHA J0836.2-7908	2002 Mar 24.5006	600	600
ECHA J0838.9-7916	2002 Mar 24.5193	600	600
ECHA J0844.2-7833	2004 Jan 10.6289	900	900

and vary with humidity and with some power of the air mass. This was particularly evident for water bands between 9300–9500 Å. Thus another correction operation is required to remove the residual  $\text{H}_2\text{O}$  absorption. We produced a water ‘map’ by first removing the  $\text{H}_2\text{O}$  features from a copy of the template spectrum, and then subtracting this edited spectrum from the original spectrum. We then produced a grid of secondary water maps, with the  $\text{H}_2\text{O}$  features scaled between 0 – 100 per cent of the original line strengths. By trial and error, the grid spectra were divided through the template-divided object spectra until few apparent  $\text{H}_2\text{O}$  features remained in the object spectra. The secondary  $\text{H}_2\text{O}$  correction needed was at the  $\pm 5 - 20$  per cent level.

The telluric-corrected spectra were extinction corrected using average values for the Siding Spring site, then pseudo-flux calibrated by comparison with spectrophotometric standard stars using the `standard`, `sensfunc` and `calibrate` routines within IRAF. Lastly, the red and blue spectra for each star were merged using the `scombine` routine and rebinned at 4 Å  $\text{pixel}^{-1}$ , producing spectra that had useful coverage for most stars from  $\lambda\lambda 3500 - 10200$  Å; see Fig. 1<sup>1</sup>.

Spectra obtained and reduced in the manner described above permit comparative spectral typing and extraction of synthetic colours and spectral indices, but not the measurement of fluxes. Other details of the spectroscopic reduction techniques employed here are discussed by Bessell (1999).

<sup>1</sup> A file containing these spectra can be downloaded from [http://www.mso.anu.edu.au/~bessell/FTP/EtaCha\\_spectra/](http://www.mso.anu.edu.au/~bessell/FTP/EtaCha_spectra/).

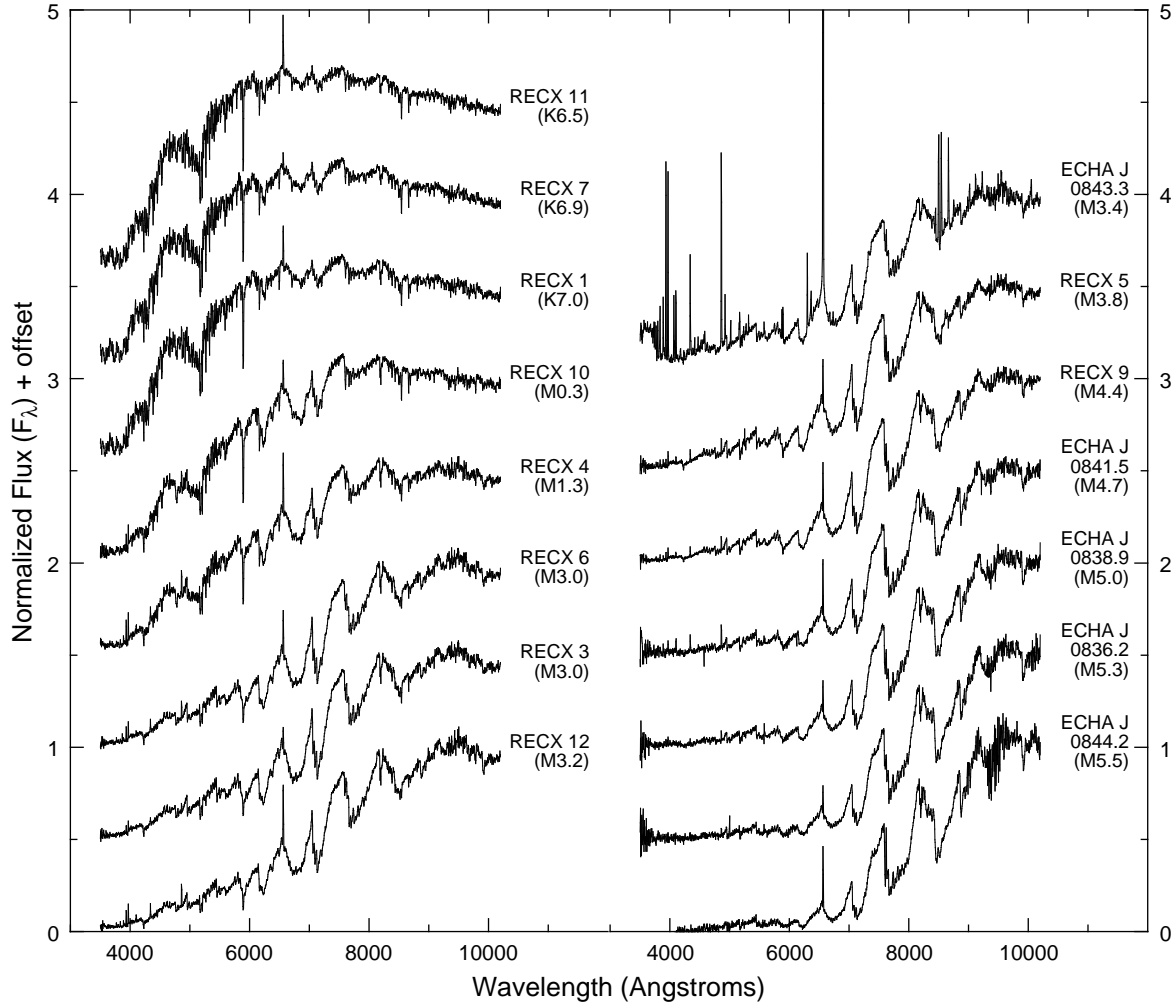


**Figure 1.** Calibrated spectra for the 15 low-mass members of the  $\eta$  Cha cluster, ordered by their adopted spectral type.

## 2.2 Derivation of the synthetic colours

We obtained synthetic colours from the flux-calibrated spectra for the 15 low-mass  $\eta$  Cha cluster stars and the Gliese dwarfs we observed. First, we obtained instrumental colours by integrating the spectra with normalized filter response functions in the Cousins  $BVRI$  system. Using published photoelectric photometry for the Gliese stars from Bessell (1990), reproduced in Table 2, we then derived transformation equations to convert the instrumental colours to the Cousins system. For all the colours, the transformation equation was a linear function with a regression coefficient  $R \approx 1$ . This transformation operation is our first evidence that the flux-calibration operation was reliable.

We can address the reliability of the synthetic colours derived for the  $\eta$  Cha cluster stars and the Gliese dwarfs in other ways; (i) comparison of the synthetic colours for the two groups of stars, the description of which occupies the majority of Section 3.1 of this paper and, (ii) comparison with published optical photometry for the  $\eta$  Cha cluster population, which we will describe here.  $VRI$  photometry

for most of the late-type  $\eta$  Cha stars, obtained with the 1-m telescope and a  $1k \times 1k$  charge-coupled device (CCD) detector at the South African Astronomical Observatory, has been published by Lawson et al. (2001), Lawson et al. (2002) and Lyo et al. (2004). Data for the Gliese dwarfs, obtained with the same telescope and instrumentation, was kindly obtained and reduced for us by L. Crause. Comparison of the synthetic and CCD colours showed an excellent correspondence for the Gliese stars. But for many of the  $\eta$  Cha stars the synthetic  $(V - I)$  colours were redder by  $\sim 0.1$  magnitudes compared to  $(V - I)$  colours at maximum light estimated from the light curves for the K- and early-M type stars. We ascribe this difference to variability; all low-mass  $\eta$  Cha stars with spectral types earlier than M5 are known photometric variables owing to the rotational modulation of cool or hot spots, and the synthetic colour was measured from a spectrum obtained at an unknown rotational phase. However, we found an excellent correspondence between the synthetic  $(R - I)$  colours, and CCD  $(R - I)$  colours derived from single-epoch observations reported by Lawson et al. (2001), Lawson et al. (2002) and Lyo et al. (2004). For most

**Table 2.**  $V$  magnitude, colours and spectral types of K- and M-type dwarfs from the Gliese catalogue (Bessell 1990), with stars identified by both their Gliese and LHS catalogue designations. The spectral types listed in the last column are derived using the spectral type-colour conversions of Bessell (1991) and Kenyon & Hartmann (1995). Only late-M stars show differences  $> 0.1$  sub-type in the derived spectral types between the two conversions; the spectral types given in brackets use the conversion of Kenyon & Hartmann (1995).

Gliese#	LHS#	$\alpha_{1950}$	$\delta_{1950}$	$V$	$(B - V)$	$(V - R)$	$(R - I)$	$(V - I)$	Sp. Type
GL 412.3	LHS 6197	11 05 43	-27 59.8	9.34	1.26	0.762	0.695	1.457	K5.8
GL 383	LHS 2231	10 09 47	-18 22.2	9.95	1.483	0.904	0.904	1.810	M0.0
GL 369	LHS 274	09 48 40	-12 04.5	10.06	1.48	0.932	1.020	1.954	M1.0
GL 429.2	LHS 2412	11 25 26	-08 53.7	12.37	1.48	0.945	1.054	2.00	M1.2
GL 382	—	10 09 46	-03 29.7	9.29	1.515	1.006	1.175	2.185	M2.1
GL 581	LHS 394	15 16 50	-07 32.4	10.57	1.616	1.101	1.409	2.508	M3.1
GL 431	LHS 2423	11 29 23	-40 46.3	11.52	1.54	1.16	1.49	2.65	M3.5
GL 375	LHS 2213	09 56 34	-46 10.7	11.29	1.533	1.146	1.512	2.657	M3.5
GL 514.1	LHS 353	13 27 29	-08 26.6	14.33	1.68	1.32	1.72	3.04	M4.3
GL 493.1	LHS 2664	12 58 05	05 57.1	13.41	1.77	1.359	1.765	3.131	M4.5
GL 473	LHS 333	12 30 51	09 17.6	12.49	1.84	1.555	1.96	3.52	M5.2(M5.1)
GL 406	LHS 36	10 54 06	07 19.2	13.53	1.99	1.856	2.177	4.032	M5.9(M5.7)
GL 283	LHS 234	07 38 02	-17 17.4	16.54	—	1.859	2.248	4.108	M6.0(M5.8)

of the late-type  $\eta$  Cha stars, the difference in the colour was  $< 0.05$  magnitudes. Those stars with colours that were different at the  $\sim 0.1$  magnitude level are dominated by objects with on-going mass accretion that have strongly-variable optical emission, especially at H $\alpha$  influencing the  $R$ -band photometry (Lawson, Lyo & Muzerolle 2004). For most of these T Tauri stars with photometric variations driven by cool starspots, we find that the  $(R - I)$  colour is largely insensitive to rotational variability. Unpublished multi-epoch  $VRI$  photometry of the  $\eta$  Cha stars, and other multi-colour rotational studies of T Tauri stars, e.g. Bouvier et al. (1993), shows  $R$ - and  $I$ -band amplitudes that are each roughly half the observed  $V$ -band amplitude. With the individual light curves appearing in-phase, the resulting  $(R - I)$  colour amplitudes are low. We therefore adopt the  $(R - I)$  colour as the primary broadband colour for characterizing the late-type  $\eta$  Cha stars since a single-epoch  $(R - I)$  measurement appears to better describe the stars than other broadband colours affected by variability, and also because the  $(R - I)$  colour has already been used to characterize the late-K and M-type dwarf spectral sequence (Bessell 1991).

### 3 SPECTRAL CLASSIFICATION OF THE LATE-TYPE POPULATION

#### 3.1 Synthetic colours – comparing the $\eta$ Cha cluster to main-sequence dwarfs

In Fig. 2 we show colour-colour diagrams for the late-type members of the  $\eta$  Cha cluster and the Gliese dwarfs (mainly old disk stars) produced using the synthetic colours derived from our calibrated DBS spectra. We also show the locus of K5 – M6 dwarfs in each of these colour-colour planes, using data compiled by Kenyon & Hartmann (1995) and Bessell (1991). In Figs 2(b) and 2(c), we see excellent agreement between the  $VRI$  synthetic colours for both groups of stars and the locus of main-sequence colours. In Fig. 2(a) we see a small but significant offset in the  $(B - V)$  colours for the  $\eta$  Cha cluster stars compared to both the sample of the Gliese stars and the dwarf colour sequence, reaching  $\approx 0.2$  magnitude for the late-M stars. This difference in  $(B - V)$  colour

might be due to a combination of several factors, in particular differences in surface gravity and metallicity, and the likelihood of enhanced chromospheric activity in young PMS populations compared to older dwarfs<sup>2</sup>. The offset is not due to variability as the late-M type cluster members have low or undetected levels of photometric variability (Lawson et al. 2002; Lyo et al. 2004). Nor is it necessarily due to the presence of an accretion disc. While the only star with a highly-discrepant  $(B - V)$  colour is the CTT star ECHA J0843.3–7905 with strong optical excess emission owing to on-going disc accretion, several other cluster members with lower levels of disc accretion are indistinguishable from the general cluster population.

Despite the difference between the  $\eta$  Cha stars and main-sequence dwarfs in the  $(B - V)$  colour, the broadband colours of the low-mass members of the  $\eta$  Cha cluster are otherwise well-matched to those of older main-sequence stars. This suggests that the spectral properties of the  $\eta$  Cha stars might be close to that of main-sequence stars.

##### 3.1.1 The CTT star ECHA J0843.3–7905

ECHA J0843.3–7905 is a CTT star with high IR excess emission of  $\Delta(K - L) = 0.9$  mag, and a mass accretion rate of  $\log \dot{M} = -9.0$   $M_{\odot} \text{ yr}^{-1}$  (Lyo et al. 2003; Lawson et al. 2004). The optical spectrum shows heightened levels of optical line and continuum emission, the star having a unique spectrum amongst the known late-type population of the cluster; see Fig. 1. The origin of the  $(B - V)$  colour excess for the star seen in Fig. 2(a) is principally due to strong  $U$ - and  $B$ -band continuum excess emission. In Fig. 3 we compare the spectrum of the star to that of a dwarf of similar spectral type (Gliese 375; spectral type M3.5) with the responses of the Cousins  $BVRI$  filters overlaid for comparison. ECHA J0843.3–7905 clearly shows excess emission at wavelengths

<sup>2</sup> A similar colour difference was noted by Stauffer (2001) when comparing the 100 Myr-old Pleiades and 700 Myr-old Praesepe cluster populations, and ascribed to differences in their metallicities and in their chromospheric activity.

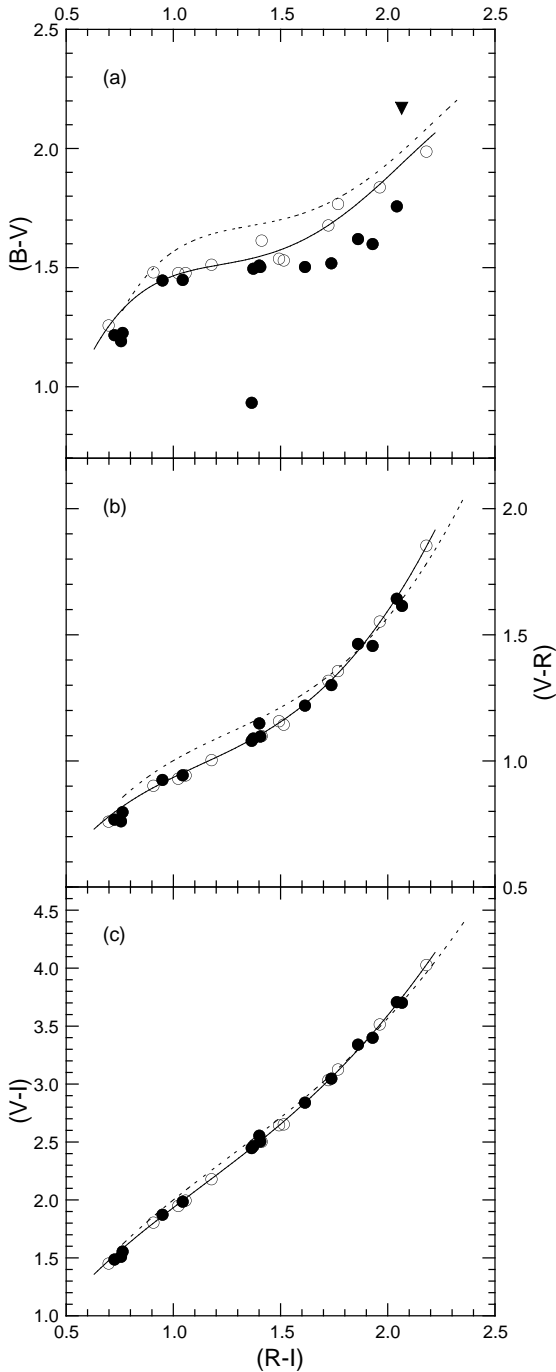


**Figure 2.** (a) Synthetic  $(B - V)/(R - I)$ , (b)  $(V - R)/(R - I)$  and (c)  $(V - I)/(R - I)$  colour-colour diagrams for  $\eta$  Cha cluster stars (filled circles) and main-sequence dwarfs (open circles). The reverse filled triangle in (a) is the faint M5 star ECHA J0844.2-7833 with a poor  $B$ -band flux. The highly-discrepant cluster observation in (a) is the CTT star ECHA J0843.3-7905 with strong  $U$ - and  $B$ -band excess emission; see Section 3.1.1 The bold lines are the locus of main-sequence stars from spectral type K5 – K6 (Kenyon & Hartmann 1995) and K7 – M6 (Bessell 1991). The dashed lines represent the effects of reddening in these colour-colour planes of  $A_V = 0.5$  mag using extinction coefficients provided by Rieke & Lebofsky (1985).

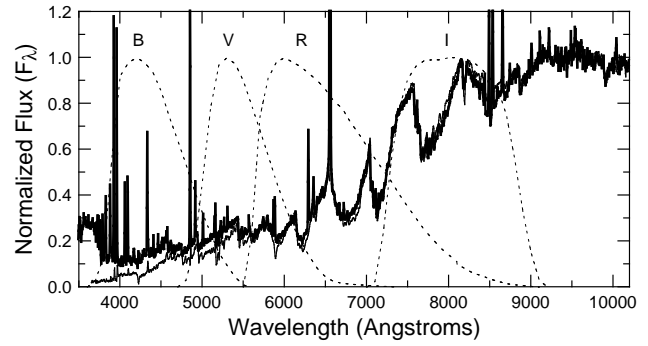


**Figure 3.** Normalized spectra of ECHA J0843.3-7905 and GL 375 (spectral type M3.5), overlaid with  $BVRI$  filter response functions in the Cousins system. ECHA J0843.3-7905 clearly shows continuum veiling, and excess continuum emission at wavelengths  $\lambda < 4000$  Å; a consequence of on-going disc accretion (Lyo et al. 2003; Lawson et al. 2004). The star also shows the rich line emission spectrum characteristic of CTT stars.

$\lambda < 4000$  Å owing to a strong Balmer continuum emission jump. Optical line emission also affects the broadband colours, in particular the contribution made by the strong  $H\alpha$  emission line to the  $R$ -band flux. If the line emission is uncorrected-for, the star has distorted broadband colours compared to other stars of similar spectral type. Editing all obvious optical emission lines from the spectrum and recalculating the colours results in a shift of  $+0.07$  and  $-0.05$  magnitudes in the  $(R - I)$  and  $(V - R)$  colours, respectively. This correction leaves the star with colours similar to other cluster stars and dwarfs of spectral type  $\approx$  M3. In Fig. 2 we plot the unmodified synthetic colours of the star, but in other figures in this paper we plot the modified  $(R - I)$  colour. From the depth of optical absorption features in the  $V$  and  $R$  bands, we estimate a veiling parameter  $r \sim 0.06$ . This low level of photospheric veiling does not appear to alter the broadband colours to a significant extent.

### 3.1.2 Reddening

The proximity of the  $\eta$  Cha cluster to Earth ( $d = 97$  pc), and the remoteness of the cluster from obscuring molecular clouds, makes it likely that interstellar reddening towards the cluster is low. Comparison of the synthetic colours for the  $\eta$  Cha cluster stars and those for the Gliese dwarfs provides us with a sensitive test for reddening, both across the region occupied by the cluster and for individual cluster members. In each panel of Fig. 2, dashed lines show the consequence of reddening of  $A_V = 0.5$  magnitudes in these colour-colour planes, employing the extinction coefficients of Rieke & Lebofsky (1985). Clearly reddening is absent or very low; no late-type member shows an offset in the colour-colour planes that could be assigned to reddening at a level exceeding a few tenths of a magnitude. We therefore adopt  $A_V = 0.0$  for the late-type stars. We further consider the issue of reddening when adopting spectral types for these stars in Section 3.3.

### 3.2 Narrow-band spectral indices

The spectral classification sequence attempts to compare stars with broadly similar spectroscopic properties across different stellar evolutionary phases, even if differences in surface gravity or chemistry are present. In Section 3.1, we found that the *VRI* colours of the  $\eta$  Cha stars are indistinguishable from old disk dwarfs. In Fig. 4(a), we compare spectra for five  $\eta$  Cha members, and five Gliese dwarfs with spectral types similar to the  $\eta$  Cha stars. Consistent with the agreement in the colour characteristics of these two groups of objects, the spectroscopic nature of these stars shows a general correspondence in appearance with similarly-strong TiO and VO bands in each pair ( $\eta$  Cha star and Gliese dwarf) of objects. However, through the application of narrow-band spectral indices we can define differences between the PMS  $\eta$  Cha stars and the main-sequence Gliese stars, which we discuss in detail in the following sections. The combination of comparative spectroscopy, and the measurement of broad-band colours and narrow band indices, will enable us to produce spectral types for the fifteen low-mass members of the  $\eta$  Cha cluster. We discuss the three early-type members in Section 4.

#### 3.2.1 Temperature-sensitive indices

Molecular bands such TiO, CaOH, CaH and VO, atomic lines such as Na I and K I, can provide temperature-sensitive information particularly for M-type stars where the appearance of the spectrum changes rapidly between sub-types; see Fig. 1. However, the usefulness of spectral indices defined to measure the change in strength of these features is constrained by their parallel sensitivity to differences in surface gravity and metallicity between the test (the  $\eta$  Cha stars) and the parent populations (the Gliese stars). In this section, we consider several narrow-band spectral indices that are principally temperature indicators as a means of supporting the comparison of the broadband colours (see Section 3.1), and of the individual spectra (Fig. 4a). Indices that appear to be useful gravity-sensitive indicators are discussed in Section 3.2.2.

We selected six temperature indices; three ‘pseudo-continuum’ (PC) spectral ratios that measure the general shape of the spectrum across restricted wavelength intervals, and indices defined from CaH, CaOH and TiO molecular band flux ratios. We adopted the PC indices from Martín et al. (1996), the CaH and CaOH indices from Reid, Hawley & Gizis (1995), and the  $[\text{TiO}]_2$  index from Kenyon et al. (1998). Table 3 lists the working definition for each index. Figs 5 and 6 compare these indices for the  $\eta$  Cha and Gliese stars against their measured ( $R - I$ ) colour. In Fig. 5, we see the PC indices are well-matched between the two groups. In Fig. 6, we see small differences in the distributions of the TiO, CaH and CaOH indices for the two groups of stars, with each group showing little scatter about the trend in index value with increasing ( $R - I$ ) colour. In Fig. 5 and each panel of Fig. 6, we fit the Gliese star data with a low-order polynomial to represent the dwarf sequence for each index. In Figs. 6(a) and (b), we see that the CaH and CaOH indices are slightly larger — corresponding to weaker molecular and strengths — in the  $\eta$  Cha cluster compared to the dwarfs of a given ( $R - I$ ) colour. Kirkpatrick, Henry

**Table 3.** Adopted spectral indices, with all wavelengths in Angstrom units. For the  $[\text{TiO}]_2$  index, the bandpass is 30 Å centred at each wavelength.

Index	Definition
Temperature-sensitive indices	
PC3	$F_{8235-8265} / F_{7540-7580}$
PC4	$F_{9190-9225} / F_{7540-7580}$
PC5	$F_{9800-9880} / F_{7540-7580}$
CaH2	$F_{6814-6846} / F_{7042-7046}$
CaOH	$F_{6230-6240} / F_{6345-6354}$
$[\text{TiO}]_2$	$-2.51 \log[F_{7100} / (0.8F_{7025} + 0.2F_{7400})]$
Gravity-sensitive indices	
NaI	$F_{8148-8172} / F_{8176-8200}$
FeH2	$F_{9840-9880} / F_{9900-9940}$
Temperature index for A-type stars	
CaII	$F_{3917-3925} / F_{3925-3942}$

& McCarthy Jr (1991) and Reid et al. (1995) showed that the CaH and CaOH molecular bands are also related to metal content, with an inverse relation between metallicity and molecular bands strength. Gizis (1997) also showed that the CaH molecular bands strength are useful to discriminate between dwarfs and subdwarfs. These results indicate that the  $\eta$  Cha cluster has slightly higher metallicity than dwarfs owing to its weaker CaH and CaOH molecular band strengths; consistent with the young age of the cluster. In Fig. 6(c), the  $[\text{TiO}]_2$  index is also larger — but this time indicating a stronger molecular band strength — in the  $\eta$  Cha cluster than in the standard dwarfs. TiO molecular bands are the main source of optical opacity in M-type stars and their strength is a well-known temperature indicator (O’Connell 1973; Solf 1978). However, the TiO molecular bands also have a small gravity dependence, e.g. Mohanty et al. (2004) showed that the TiO triple-headed bands ( $\lambda 8432, 8442, 8452$ ) become stronger with decreasing gravity. Therefore we suggest that the difference in the  $\lambda 7100$  TiO molecular band strength is a function of lower gravity in the  $\eta$  Cha cluster compared to the main-sequence stars, again consistent with the PMS nature of the cluster.

#### 3.2.2 Gravity-sensitive indices

In Fig. 4(a) we compared spectra for five  $\eta$  Cha members, with five Gliese dwarfs with similar spectral types to the  $\eta$  Cha stars. A visual assessment of these spectra confirms their similarity, supported by the measurement of the PC and molecular band indices discussed above. However, in detail we see slight differences between the two groups of spectra in gravity sensitive features, e.g. the  $\lambda 7665, 7699$  K I doublet, the  $\lambda 8183, 8195$  Na I doublet, and the  $\lambda 9896$  FeH bandhead (O’Connell 1973; Kirkpatrick et al. 1991; Martín et al. 1996). In Fig. 4(b) we illustrate the difference in these lines by producing ratios of the spectra, where the spectrum of each  $\eta$  Cha star is divided by the spectrum of the Gliese star of the nearest spectral type. Small differences of  $< 1$  sub-type in the spectral types, and slightly stronger TiO bands in the  $\eta$  Cha stars, leave low-level residual TiO and VO features. But the ratioed spectra are dominated by resid-

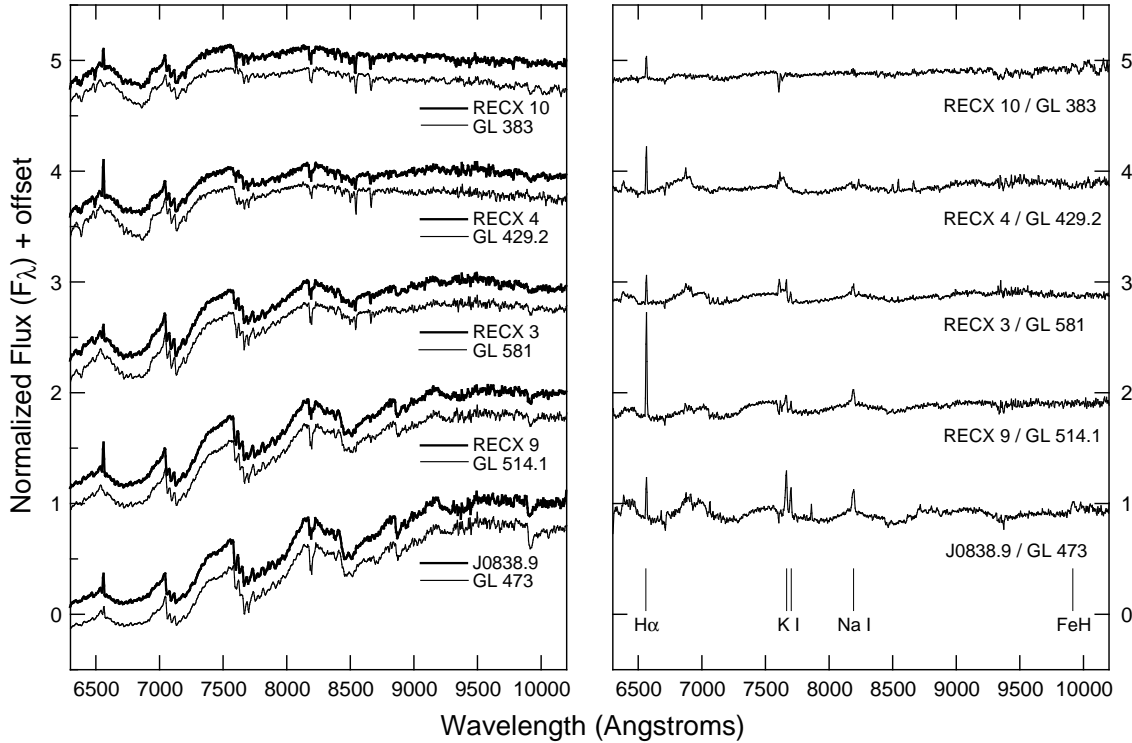


**Figure 4.** (a) Comparison of  $\eta$  Cha cluster members and Gliese dwarfs of similar spectral types, as determined from their broadband colours: RECX 10 and GL 383 (spectral type  $\approx$  M0), RECX 4 and GL 429.2 ( $\approx$  M1), RECX 3 and GL 581 ( $\approx$  M3), RECX 9 and GL 514.1 ( $\approx$  M4) and ECHA J0838.9–7916 and GL 473 ( $\approx$  M5). (b) Ratioed spectra obtained by dividing the cluster star spectrum by the dwarf spectrum. Positive residuals indicate the  $\eta$  Cha star has weaker absorption features than the dwarf. H $\alpha$  also appears as a positive residual as it is in emission in the  $\eta$  Cha stars. While the overall spectroscopic properties of the two groups of stars are very similar, small differences in band strengths (due to slight mis-matches in spectral type, as well as intrinsic variations between the two groups of stars) and significant differences in gravity-sensitive features are evident; see Section 3.2 for details.

uals owing to significant differences in the strengths of the K I, Na I and FeH lines. Positive residuals indicate the features are weaker in the  $\eta$  Cha stars compared to the dwarfs. (H $\alpha$  appears as a strong positive residual, owing to this feature being in emission in all of the late-type  $\eta$  Cha stars.) In Fig. 4(b) we see positive K I doublet residuals from RECX 4 (spectral type M1), clear evidence for positive Na I doublet residuals from RECX 3 (M3), and FeH residuals for ECHA J0838.9–7916 (M5). For quantitative comparison of the Na I doublet and the FeH bandhead in these stars, we used a line index that compares the line fluxes to nearby pseudo-continuum points. For the FeH lines, we adopted the FeH2 ratio of Martín et al. (1999) and we followed their technique to define the Na I ratio. Table 3 lists the working definition for each index. In Fig. 7 we show these index values for the  $\eta$  Cha cluster stars, together with the Gliese stars, and values for M-type giants derived using spectra published by Pickles et al. (1998). Both indices clearly differentiate the  $\eta$  Cha stars from dwarfs and giants, with the T Tauri stars having intermediate gravity indicators consistent with the elevation of the cluster a few magnitudes above the main sequence.

### 3.3 Adopted spectral types for the late-type stars

Table 4 lists the synthetic colours, and spectral types for the fifteen low-mass members of the  $\eta$  Cha cluster derived from their low-resolution spectra by comparison to standard dwarfs with known spectral types via their broadband  $VRI$  colours – represented in Table 4 by the  $(R - I)$  colour (Figs 2b and c), the average of the three PC ratios (Fig 5), and the CaH and TiO molecular bands strengths (Figs 6a and 6c). The adopted spectral types for these stars (last column of Table 4) are roughly an average of these values, with emphasis given to the very-similar  $(R - I)$  and PC results. For the K-type and M0 stars, spectral types derived from the  $(R - I)$  colour and PC indices are in agreement only at the 0.5 – 1 sub-type level because these indices vary slowly with K sub-type. For the later M-type stars, the agreement is at the 0.2 sub-type level. However, spectral types derived from CaH2 index are  $\approx$  0.3 sub-types earlier compared with those from the  $(R - I)$  colour, while those derived from the [TiO]<sub>2</sub> index are  $\approx$  0.3 sub-types later. The differences seen in the CaH2 and [TiO]<sub>2</sub> indices are consistent with the PMS  $\eta$  Cha cluster having higher metallicity (derived from the CaH2 index) and lower surface gravity (derived from the [TiO]<sub>2</sub> index) than the Gliese dwarfs; see Section 3.2.1 for details. The opposite effects of the CaH2 and [TiO]<sub>2</sub> indices result in an average spectral type not very different from

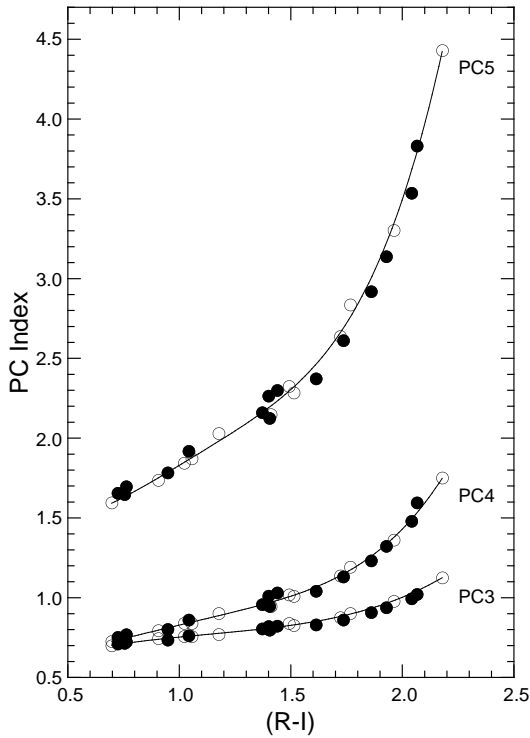


**Figure 5.** PC3, PC4 and PC5 spectral indices for  $\eta$  Cha cluster stars (filled circles) and main-sequence dwarfs (open circles), with the solid lines being low-order fits to the dwarf data. For all three PC indices, the distributions for the  $\eta$  Cha cluster are well-matched to those of the dwarfs.

that derived solely from the broadband colours and the PC indices. Overall, the adopted spectral types listed in Table 4 are uncertain by 0.25 – 0.5 sub-types for the K-type stars, reducing to 0.1 – 0.2 sub-types for the M-type stars<sup>3</sup>.

The similarity of the derived spectral types from the broadband colours, the PC ratios, and the narrow line indices, further supports a lack of reddening for these stars (see Section 3.1.2). Also, a number of these stars are confirmed (RECX 1, 7, 9 and 12) or suspected (ECHA J0836.2–7908 and ECHA J0838.9–7916) binaries. All of these systems have low mass ratios of  $< 3 : 1$  (Lyo et al. 2004), with the secondary appearing to cause little or no apparent distortion of the synthetic colours or spectral indices of the primary.

#### 4 SPECTRAL CLASSIFICATION OF THE EARLY-TYPE POPULATION

For the early-type stars, Westin (1985) found  $E(b - y) = -0.004$  for  $\eta$  Cha (spectral type B8), and the light curve of the binary RS Cha (A7 + A8) has been modelled assuming

<sup>3</sup> Our adopted spectral types are similar to those previously derived for the  $\eta$  Cha cluster, e.g. from medium resolution H $\alpha$ -region spectroscopy (Mamajek et al. 1999), ( $V - I$ ) photometry (Lawson et al. 2001) and uncalibrated low resolution  $R$ -band spectroscopy (Luhman & Steeghs 2004). The principal difference is that our spectral types for the K-type stars are 1 – 2 sub-types later than the other studies, but there is agreement at  $< 0.5$  sub-types for most of the M-type stars.

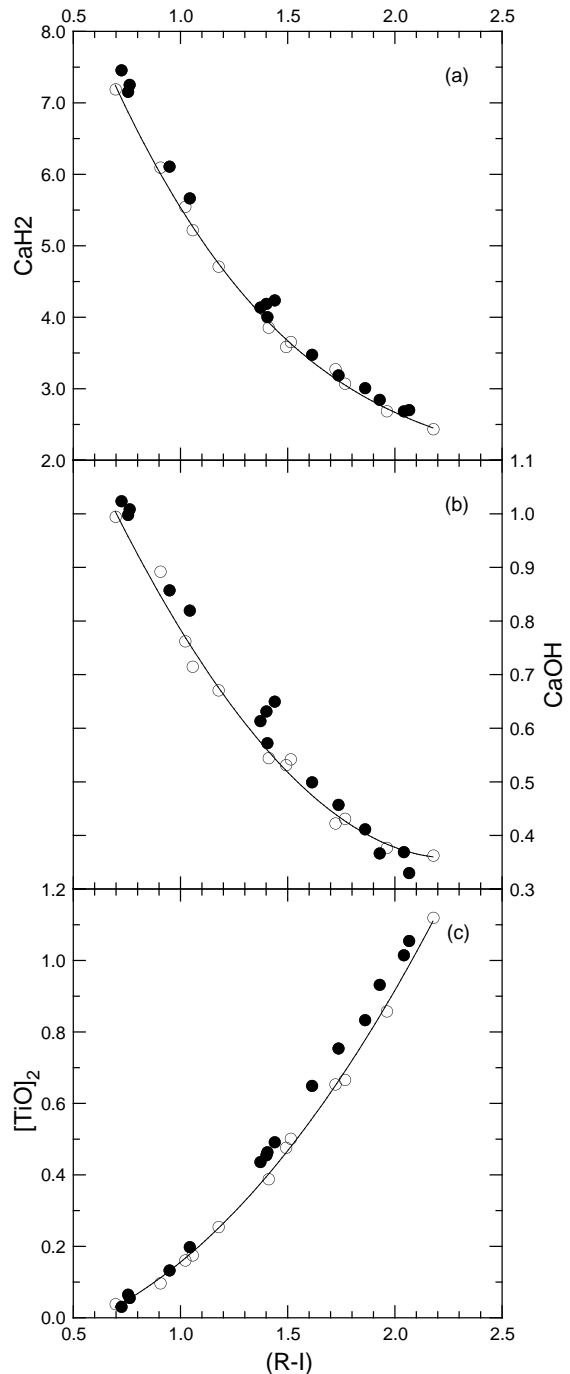


**Figure 6.** (a) CaH2, (b) CaOH, (c) [TiO]<sub>2</sub> spectral indices for the  $\eta$  Cha cluster (filled circles), and standard main-sequence stars (open circles). In panels (a) and (b), the most-discrepant cluster member is ECHA J0843.3–7905, with unusual CaH2 and CaOH indices owing to low levels of photospheric veiling.

$E(B - V) = 0.0$ , e.g. Clausen & Nordström (1985). However, for HD 75505 there is inconsistency between the spectral type of A1 given by Houk & Cowley (1975) and photometric colours that suggest a spectral type of A5–A6 (Mamajek et al. 1999), leading to dispute between Mamajek et al. (2000) and Luhman (2001) whether the star is misclassified or if it

**Table 4.** Synthetic colours for the late-type  $\eta$  Cha cluster stars derived from the low-resolution spectra, ordered by their adopted spectral types. Spectral types are derived from comparison with dwarfs from the broadband *VRI* colours, represented here by the  $(R - I)$  colour, the average of the three pseudo-continuum spectral ratios and two indices representing the CaH and TiO molecular bands strengths; see Section 3. For ECHA J0843.3-7905, the values in brackets were obtained following the removal of all obvious emission lines from the spectrum. The final column of the table lists our adopted spectral types for these stars; see Section 3.3 for details.

Star	Synthetic Colours				Spectral Types				
	$(B - V)$	$(V - I)$	$(V - R)$	$(R - I)$	$(R - I)$	PC	CaH2	[TiO] <sub>2</sub>	Adopted
RECX 11	1.22	1.49	0.77	0.72	K6.3	K7.3	<K5.8	<K5.8	K6.5
RECX 7	1.19	1.51	0.76	0.75	K6.8	K7.3	<K5.8	K7.7	K6.9
RECX 1	1.23	1.56	0.80	0.76	K6.8	K8.5	K5.8	K7.0	K7.0
RECX 10	1.45	1.88	0.93	0.95	M0.3	K9.9	M0.0	M0.6	M0.2
RECX 4	1.45	1.99	0.95	1.04	M1.2	M1.4	M0.8	M1.5	M1.3
RECX 6	1.50	2.47	1.09	1.37	M3.0	M3.1	M2.8	M3.3	M3.0
RECX 3	1.51	2.51	1.10	1.40	M3.1	M3.0	M2.9	M3.4	M3.0
RECX 12	1.51	2.56	1.15	1.40	M3.1	M3.4	M2.7	M3.4	M3.2
ECHA J0843.3-7905	0.94(1.10)	2.45(2.47)	1.08(1.03)	1.36(1.44)	(M3.3)	M3.5	M2.7	M3.5	M3.4
RECX 5	1.51	2.84	1.22	1.61	M3.9	M3.7	M3.8	M4.3	M3.8
RECX 9	1.52	3.05	1.30	1.73	M4.4	M4.2	M4.4	M4.8	M4.4
ECHA J0841.5-7853	1.62	3.35	1.47	1.86	M4.8	M4.6	M4.6	M5.1	M4.7
ECHA J0838.9-7916	1.60	3.41	1.46	1.93	M5.1	M4.9	M4.9	M5.4	M5.0
ECHA J0836.2-7908	1.76	3.71	1.65	2.04	M5.4	M5.3	M5.2	M5.6	M5.3
ECHA J0844.2-7833	2.17:	3.71	1.62	2.06	M5.5	M5.5	M5.2	M5.7	M5.5

is extinguished by  $A_V \approx 0.4$  magnitudes. To resolve the issue, we obtained DBS spectra of the three early-type cluster members along with A- and B-type dwarfs from the Bright Star Catalog. We characterized the spectra by defining a spectral index comparing the strength of the  $\lambda 3934$  Ca II line with respect to the nearby pseudo-continuum; see Table 3. Within an uncertainty of  $\approx 0.5$  subtypes we confirm the published spectral types for the three early type cluster members, indicating that HD 75505 is reddened. The reddening towards HD 75505 must be confined to the star as other nearby cluster members appear to be unextinguished. The reddening is likely associated with an edge-on disc; Lyo et al. (2003) found that HD 75505 has a  $(K - L)$  excess of  $\approx 0.2$  magnitudes.

## 5 NEW COLOUR-MAGNITUDE DIAGRAMS FOR THE $\eta$ CHA CLUSTER

PMS evolutionary models are an important tool to determine the ages and masses of the members of young stellar populations and thus are critical for star formation studies. However, there are large variations between different PMS models because of differences in the treatment of convection, deuterium burning and opacity in young stars. The resulting differences in evolutionary grids result in a wide range of inferred ages and masses for individual objects, e.g. Lawson & Feigelson (2001) compared the late-type members of the  $\eta$  Cha to several PMS grids and found differences of 1.5 – 4 in the derived age and/or mass for individual stars.

There are two main ways to test the validity of PMS grids. First, accurate dynamical masses and modelled temperatures and luminosities of components of dual-lined spectroscopic/eclipsing binaries can be directly compared to the grids. In the  $\eta$  Cha cluster, the only known dual-lined eclipsing system is the early-type binary RS Cha AB. The majority of contemporary PMS grids infer an age  $t \approx 8.5$  Myr for

this system, with  $\Delta t = 0.5 - 1$  Myr owing to uncertainties in the temperature and luminosity of the components (Mama-jek et al. 2000; Lawson & Feigelson 2001; Young et al. 2001). Secondly, older PMS systems can be used to check for coevality across the extent of the stellar population. For PMS cluster ages  $t > 5 - 10$  Myr, a spread of ages of a few Myr within a stellar group corresponds to an almost negligible range of luminosities for any given stellar mass. The main contributor to the width of the locus for an older cluster is unresolved binaries that appear overly luminous compared to single stars (Lawson et al. 2001; Luhman 2001).

Lyo et al. (2004) showed that the scatter of magnitude in the  $V/(V - I)$  color-magnitude (C-M) diagram for the  $\eta$  Cha cluster is due to binaries confirmed for several stars by speckle imaging (RECX 1 and RECX 9; Köhler & Petr-Gotzens 2002), radial velocity variability (RECX 7; Lyo et al. 2003) and light curve analysis (RECX 12; Lawson et al. 2001). Binarity is strongly suspected for other late-type stars owing to their elevation in the C-M diagram. All of these systems appear to have low mass ratios of  $< 3 : 1$  appearing up to 0.7 magnitudes, corresponding to a factor of 2 in brightness, above the locus of apparently single stars. With binarity in the late-type population accounted for, the scatter in the C-M diagram is considerably reduced, indicating that the stars form an essentially coeval, natural isochrone.

The analysis of Lawson & Feigelson (2001) did not include five M-type stars recently discovered in area photometric surveys aimed at defining the low-mass cluster population (Lawson et al. 2002; Lyo et al. 2004; Song et al. 2004). While an extensive comparison between the low mass stellar population of the cluster and the numerous PMS grids available in the literature is not the aim of this paper, in Fig. 8 we compare in the  $I/(R - I)$  C-M diagram the cluster stars to the grids of (a) Siess, Dufour & Forestini (2000) and (b) Baraffe et al. (1998). Both grids provide users with absolute magnitudes in the standard photometric bands for direct comparison with observable quantities. We adopt the

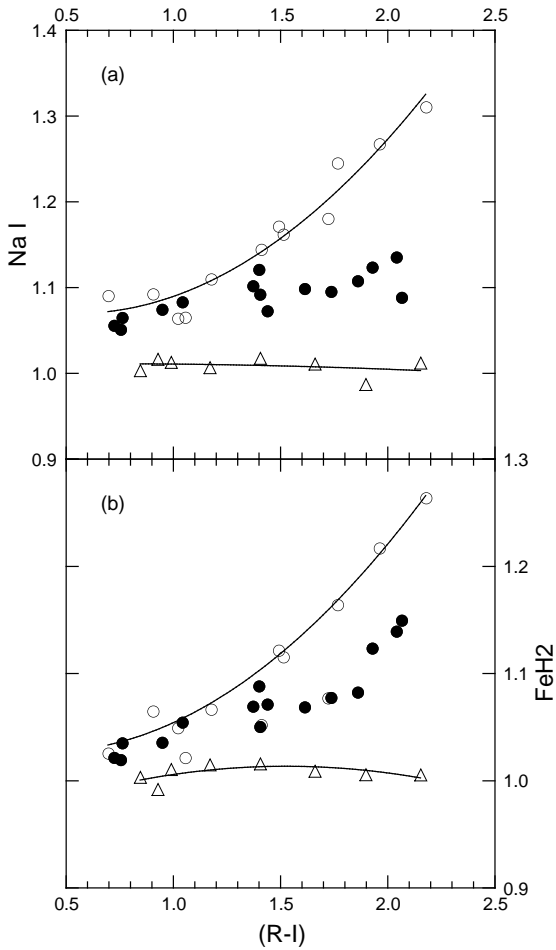


**Figure 7.** Comparison of gravity-sensitive indices measuring the strength of (a) the  $\lambda 8183, 8195$  Na I doublet, and (b) the  $\lambda 9896$  FeH band for the  $\eta$  Cha cluster (filled circles), old disk dwarfs (open circles) and giants (open triangles). For both indices the distribution for  $\eta$  Cha cluster stars occupies the region between that of the dwarfs and the giants.

$I/(R-I)$  C-M diagram in this paper because we use the  $(R-I)$  colour to define the spectral types of the cluster population. The  $(R-I)$  colours are taken from Table 4. For the  $I$ -band magnitudes, we derive values from Lawson et al. (2001) and Lyo et al. (2004), and we adopt the DENIS  $i$ -band measurement for the faint M5.5 star ECHA J0844.2–7833. As we explain in Section 3.1,  $(R-I)$  is the optical broadband colour least-affected by variability, and for most of these stars the published  $I$ -band magnitude is approximately the brightness at maximum light. This represents the least-spotted case for stars with cool starspots, but might give too bright a magnitude for stars with variability driven by accretion hotspots, such as the CTT star ECHA J0843.3–7905.

For the K- and early M-type stars with  $(R-I) < 1.5$ , the inferred masses and ages of the  $\eta$  Cha cluster stars in the  $I/(R-I)$  C-M diagram is similar to that inferred from the  $V/(V-I)$  C-M diagram with some differences in detail for individual stars, e.g. in Fig. 8(a), the grid of Siess et al. (2000) infers an age for the stars (we take the lower

locus to represent single stars) of 7–9 Myr. A similar result is obtained from the  $V/(V-I)$  C-M diagram (Lawson & Feigelson 2001). However, the  $I/(R-I)$  C-M plane gives slightly lower inferred masses than from the  $V/(V-I)$  C-M plane. But these small differences in mass and age for individual stars are minor when compared to problems raised when exposing the grids to the full range of spectral types present in the cluster, and the extreme differences seen when comparing different grids.

First, while the grids of Siess et al. (2000) approximately achieves coevality for spectral types earlier than  $\approx$  M3.5, later-type stars appear systematically older. The same problem with these grids was noted by Feigelson, Lawson & Garmire (2003) for the younger ( $t = 5$  Myr) PMS group of late-type stars associated with  $\epsilon$  Cha and HD 104237. Secondly, the grids of Baraffe et al. (1998) fail to achieve coevality across any significant range of colour/spectral type owing to known problems with the optical fluxes for these models. Third, there is almost no agreement between the two sets of grids concerning the inferred age and mass for individual stars. The obvious problems with the Baraffe et al. (1998) models appear to be somewhat alleviated in the H-R (luminosity-temperature) diagram (Lawson & Feigelson 2001) but these grids still infer a somewhat older age for the cluster ( $t \sim 15$  Myr) than that inferred from the Siess et al. (2000) grids ( $t \sim 9$  Myr).

This two-model comparison amply demonstrates that the  $\eta$  Cha cluster is a demanding laboratory for the predictions of PMS evolutionary models. To assist the development of future PMS grids, in Table 5 we list optical photometric data for spectral types of K7 – M5.5 that represent the observed cluster isochrone. The values for  $M_V$  are derived from C-M diagrams for the cluster such as Fig. 8, with the isochrone fitted to those stars that appear to be single stars, or undetected high-mass ratio binaries; also see Lawson & Feigelson (2001) and Lyo et al. (2004). The observed  $V$ -band magnitudes are converted to absolute magnitudes *via* the distance modulus of 4.93, determined from the distance to the cluster of  $d = 97 \pm 3$  pc (Mamajek et al. 1999). The  $(B-V)$  colours are derived from the observed sequence of  $\eta$  Cha stars in Fig. 2(a), while for the  $(V-R)$ ,  $(V-I)$  and  $(R-I)$  colours we adopt the dwarfs colours of Bessell (1991) since the  $VRI$  colours of the late-type  $\eta$  Cha closely follow the dwarf sequence (Figs 2b and c). The colour sequences are well-defined for the cluster stars, and for individual spectral types the colours are likely to be uncertain by only 0.01–0.02 magnitudes. The values for  $M_V$  are imprecise owing to the subjective nature of the fit to stars in the C-M plane, issues of variability and undetected binarity, and uncertainty in the distance modulus (which alone contributes a zero-point uncertainty of 0.06 magnitudes). Altogether, the values for  $M_V$  may be uncertain by 0.1 – 0.2 magnitudes.

## 6 SUMMARY AND CONCLUSIONS

Comparison of the  $\approx 9$  Myr-old  $\eta$  Cha cluster PMS stars to Gyr-old main-sequence K- and M-type dwarfs demonstrates the high degree of similarity of the spectra of these two groups of objects. Broadband  $VRI$  colours and pseudo-continuum indices derived for the cluster stars and dwarfs from flux-calibrated low resolution spectra are indistinguish-

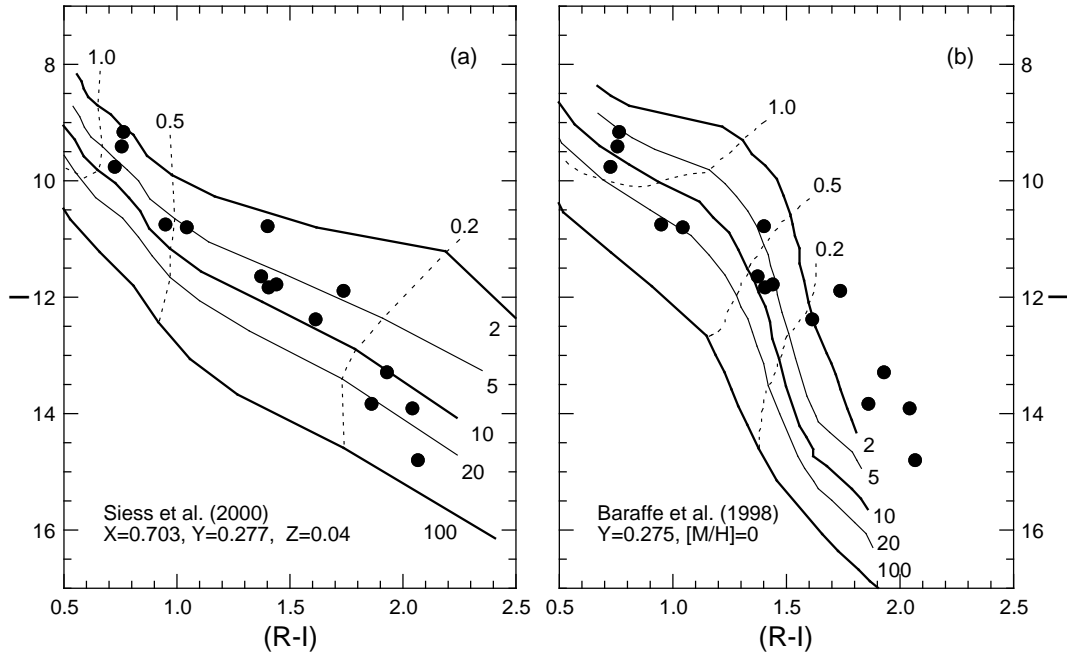


**Figure 8.** *RI* colour-magnitude diagram for the low-mass members of the  $\eta$  Cha cluster compared to the pre-main sequence grids of (a) Siess et al. (2000) and (b) Baraffe et al. (1998). Iso-mass lines are in units of  $M_{\odot}$ ; isochrones are in units of Myr. When shown in these diagrams to their full extent, the iso-mass lines extend from ages of 1 – 100 Myr and the isochrones run across masses of 0.1 – 1.4  $M_{\odot}$ .

**Table 5.** Optical photometry representing the  $\eta$  Cha cluster isochrone for single stars, with the *V*-band magnitudes placed on the absolute scale.

Sp. Type	$M_V$	$(B - V)$	$(V - R)$	$(V - I)$	$(R - I)$
K7	6.67	1.26	0.83	1.60	0.77
M0	7.47	1.41	0.89	1.80	0.91
M1	7.93	1.46	0.94	1.96	1.02
M2	8.43	1.48	1.00	2.16	1.16
M3	9.24	1.50	1.10	2.47	1.37
M4	10.48	1.51	1.23	2.86	1.63
M5	12.36	1.66	1.48	3.39	1.91
M5.5	13.61	1.77	1.69	3.75	2.06

able at visual and red wavelengths ( $\lambda\lambda = 5000 - 10000$  Å); see Section 3.1. This outcome suggests the temperature sequence for the  $\eta$  Cha cluster stars is not very different from that of the dwarf sequence. Aided by comparative spectroscopy between the two groups of stars, we use these indices as primary diagnostics of spectral type, with the various colours and indices in agreement at the 0.1 – 0.2 subtype level for M-stars, and at the < 0.5 subtype level for K-stars (Section 3.3).

Only in the *B*-band and for narrow-band spectral indices sensitive to metallicity and gravity, are we consistently able to differentiate the cluster stars from the dwarf stars (Sections 3.1 and 3.2). The PMS stars show a *B*-band excess of < 0.1 magnitudes for K- and early M-type stars, with the excess attaining  $\approx 0.2$  magnitudes for M4–M5 cluster members. We ascribe the *B*-band excess to at least one of three contributing factors – lower effective gravity, higher metal-

licity and enhanced optical activity. Indices that measure the temperature-sensitive CaH and TiO molecular bands strengths show that the  $\eta$  Cha stars are subtly different from dwarfs, with small but consistent deviations from the dwarf sequence that we interpret as evidence that these indices are secondary metallicity and gravity indicators. The CaH and TiO indices suggest higher metallicity and lower effective gravity in the cluster stars, respectively. Gravity-sensitive indicators, such as the K I and Na I atomic lines and the FeH molecular line, clearly locate the  $\eta$  Cha cluster between the locus of dwarfs and that of giants. While the indices derived from the low-resolution spectra show consistent behavior, in particular their sensitivity to gravity, they do not permit a precise quantitative measure of the metallicity or gravity which awaits future high-resolution study.

The outcomes described above are consistent with the location of the  $\eta$  Cha cluster in the H-R (or C-M) diagram. The ‘intermediate’ age of the stellar population positions the cluster isochrone almost equally between that of the youngest PMS populations (with ages  $\approx 1$  Myr) and the main-sequence. The general nature of the spectra are very similar to dwarfs, but the possible indication of higher metallicity and the strong indication of lower gravity is consistent with the comparative youth of the  $\eta$  Cha cluster.

With a known population of 18 primaries spanning spectral types of B8–M5.5, the  $\eta$  Cha cluster is a demanding laboratory for PMS evolutionary grids. In Section 5 we compare the cluster to two recent calculations (Baraffe et al. 1998; Siess et al. 2000) in the  $I/(R - I)$  C-M diagram and we find that both grids fail a test for coevolution for spectral types later than M3–M4. Making use of our adopted spectral types and broadband photometry, we observationally define the cluster isochrone for  $\sim 9$  Myr-old PMS stars

across spectral types of K7–M5.5. The future discovery of other low mass cluster members might usefully extend this isochrone to the lowest stellar masses and into the brown dwarf regime; IMF calculations by Lyo et al. (2004) suggest  $\sim 20$  undetected low mass stars and brown dwarfs could accompany the known stellar population.

## ACKNOWLEDGMENTS

ARL acknowledges the support of a UNSW@ADFA International Postgraduate Research Scholarship. WAL's research is supported by UNSW@ADFA Faculty and Special Research Grants. We thank Lisa Crause for obtaining photometry for this paper, Steve James and Eric Feigelson for assistance at the telescope, and the MSSSO time allocation committee for 2.3-m/DBS time during 2002 – 2004. We also thank the referee for their helpful comments.

## REFERENCES

- Baraffe I., Chabrier G., Allard F., Hauschildt P. H., 1998, *A&A*, 337, 403
- Bessell M. S., 1990, *A&ASS*, 83, 357
- Bessell M. S., 1991, *AJ*, 101, 662
- Bessell M. S., 1999, *PASP*, 111, 1426
- Bouvier J., Cabrit S., Fernández M., Martín E. L., Matthews J. M., 1993, *A&A*, 272, 176
- Clausen J., Nordström B., 1985, *A&A*, 83, 339
- Feigelson E. D., Lawson W. A., Garmire G. P., 2003, *ApJ*, 599, 1207
- Gizis J. E., 1997, *AJ*, 113, 806
- Houk N., Cowley A., 1975, *Catalogue of Two-Dimensional Spectral Types for HD Stars*, University of Michigan, Ann Arbor
- Kenyon S. J., Brown D. I., Tout C. A., Berlind P., 1998, *AJ*, 115, 2491
- Kenyon S. J., Hartmann L., 1995, *ApJSS*, 101, 117
- Kirkpatrick J. D., Henry T. J., McCarthy Jr. D. W., 1991, *ApJSS*, 77, 417
- Köhler R., Leinert C., 1998, *A&A*, 331, 977
- Lawson W. A., Crause L. A., Mamajek E. E., Feigelson E. D., 2001, *MNRAS*, 321, 57
- Lawson W. A., Crause L. A., Mamajek E. E., Feigelson E. D., 2002, *MNRAS*, 329, L29
- Lawson W. A., Feigelson E. D., 2001, in Montmerle T., André P, eds, *ASP Conf. Series Vol. 243, From Darkness To Light*, Astron. Soc. Pac., San Francisco, p. 591
- Lawson W. A., Lyo A-R., Muzerolle J., 2004, *MNRAS*, 351, L39
- Luhman K. L., 2001, *ApJ*, 560, 287
- Luhman K. L., Steeghs D., 2004, *ApJ*, 609, 917
- Lyo A-R., Lawson W. A., Mamajek E. E., Feigelson E. D., Sung E-C., Crause L. A., 2003, *MNRAS*, 338, 616
- Lyo A-R., Lawson W. A., Feigelson E. D., Crause L. A., 2004, *MNRAS*, 347, 246
- Mamajek E. E., Lawson W. A., Feigelson E. D., 1999, *ApJ*, 516, L77
- Mamajek E. E., Lawson W. A., Feigelson E. D., 2000, *ApJ*, 544, 356
- Martín E. L., Delfosse X., Basri G., Goldman B., Forveille T., Zapatero Osorio M. R., 1999, *AJ*, 118, 2466
- Martín E. L., Rebolo R., Zapatero-Osorio M. R., 1996, *ApJ*, 469, 706
- Mohanty S., Basri G., Jayawardhana R., Allard F., Hauschildt P., Ardila D., 2004, *ApJ*, 609, 854
- O'Connell R. W., 1973, *AJ*, 78, 1074
- Pickles A. J., 1998, *PASP*, 110, 863
- Reid I. N., Hawley S. L., Gizis J. E., 1995, *AJ*, 110, 1838
- Rieke G. H., Lebofsky M. J., 1985, *ApJ*, 288, 618
- Siess L., Dufour E., Forestini M., 2000, *A&A*, 358, 593
- Solf J., 1978, *A&AS*, 34, 409
- Song I., Zuckerman B., Bessell M. S., 2004, *ApJ*, 600, 1016
- Stauffer J. R., 2001, in Jayawardhana R., Greene T. P., eds, *ASP Conf. Ser. Vol. 244, Young Stars Near Earth: Progress and Prospects*, p. 127
- Westin T. N. G., 1985, *A&AS*, 60, 99
- Young P. A., Mamajek E. E., Arnett D., Liebert J., 2001, *ApJ*, 556, 230

This paper has been typeset from a  $\text{\TeX}$ / $\text{\LaTeX}$  file prepared by the author.